

# Differential thermal analysis and solution growth of intermetallic compounds

Y. Janssen <sup>a,b,\*</sup> M. Angst <sup>a</sup> K.W. Dennis <sup>b</sup> R.W. McCallum <sup>b</sup>  
P.C. Canfield <sup>a,c</sup>

<sup>a</sup>*Condensed Matter Physics, Ames Laboratory, 50011 Ames IA*

<sup>b</sup>*Materials and Engineering Physics, Ames Laboratory, 50011 Ames IA*

<sup>c</sup>*Department of Physics and Astronomy, Iowa State University, 50011 Ames IA*

---

## Abstract

To obtain single crystals by solution growth, an exposed primary solidification surface in the appropriate, but often unknown, equilibrium alloy phase diagram is required. Furthermore, an appropriate crucible material is needed, necessary to hold the molten alloy during growth, without being attacked by it. Recently, we have used the comparison of realistic simulations with experimental differential thermal analysis (DTA) curves to address both these problems. We have found: 1) complex DTA curves can be interpreted to determine an appropriate heat treatment and starting composition for solution growth, without having to determine the underlying phase diagrams in detail. 2) DTA can facilitate identification of appropriate crucible materials. DTA can thus be used to make the procedure to obtain single crystals of a desired phase by solution growth more efficient. We will use some of the systems for which we have recently obtained single-crystalline samples using the combination of DTA and solution growth as examples. These systems are TbAl, Pr<sub>7</sub>Ni<sub>2</sub>Si<sub>5</sub>, and YMn<sub>4</sub>Al<sub>8</sub>.

*Key words:* A1. Thermal analysis, Solidification, A2. Growth from high-temperature solutions, Single crystal growth, B1. Rare-earth compounds

---

## 1 Introduction

Solution growth emulates a way in which nature often produces single crystals of minerals, i.e. out of a liquid with a composition that is different from the

---

\* Corresponding author.

*Email address:* yjanssen@ameslab.gov (Y. Janssen).

product [1,2,3]. In our laboratory, as well as in others, many of the materials that are produced for investigations of their physical properties, are grown as single crystals by solution growth. Often, when it comes to producing single crystals of a desired phase, insufficient phase-diagram data is available, and we must estimate which composition and temperature ranges may produce the desired phase as well as what crucible to use. Then, based on the products of such experiments, it is decided if and how to alter the the initial composition, temperature range and crucible material. This process can, at times, require multiple iterations that consume both time and resources.

Recently, we have expanded the use of differential thermal analysis (DTA) as part of this procedure. We have found that the use of DTA can greatly facilitate the optimization of the growth, and can play a role in selecting the right crucible material. In this paper, which is focussed on solution growth, the comparison of realistic simulations with experimental differential thermal analysis (DTA) curves is used to obtain growth parameters without detailed knowledge of phase diagrams, whereas prior use of DTA for crystal growth mainly involved detailed and lengthy phase-diagram studies (see e.g. Ref. [4]).

In the following, after describing the experimental techniques, we will present simulations of DTA signals for a hypothetical binary system. Then we will discuss the DTA-assisted growth of three compounds that may serve as examples: TbAl, Pr<sub>7</sub>Ni<sub>2</sub>Si<sub>5</sub>, and YMn<sub>4</sub>Al<sub>8</sub>. Of these phases, mm-sized single crystals have not been produced before.

The descriptions of solution growth in this paper are by no means complete. Rather, with its focus is on the use of DTA for determining solution-growth parameters, it should be considered an extension to earlier papers, by Fisk and Remeika [1], Canfield and Fisk [2] and Canfield and Fisher [3].

## 2 Experimental

Differential thermal analysis (DTA) was performed in a PerkinElmer Pyris DTA 7 differential thermal analyzer. As a process gas, we used Zr-gettered ultra-high-purity Ar. For crucibles we used Al<sub>2</sub>O<sub>3</sub> (manufactured by PerkinElmer), MgO (custom-made by Ozark Technical Ceramics, Inc.), and Ta (home-made from small-diameter Ta tubes). In order to protect the Pt cups and the thermocouple of our instrument from possible Ta diffusion, the Ta crucibles were placed inside standard ceramic crucibles. The samples, with mass  $\sim$ 40-80 mg, were made by arc melting appropriate amounts of starting materials with typical (elemental) purities of 99.9-99.99%. An experiment consisted of two or three cycles at heating and cooling rates of typically 10-40°C/min. The data from the first heating cycle was different from data from subsequent heating

cycles. This may have occurred because the sample shape did not conform to the crucible so that it was not in intimate contact with the crucible walls until it had melted, or because a reaction with the crucible changed the composition of the sample. In a DTA curve, besides the events described in Sec. 3, there is also a baseline, not associated with the properties of the sample (see e.g. Ref. [5]). This baseline is also influenced by the rate at which the DTA-unit ramped.

For the growth experiments we used the following procedure [1,2,3]. Appropriate amounts of starting materials with typical (elemental) purities of 99.9-99.99% were selected, pre-alloyed by arc melting, if needed, and put into a crucible. The crucible material was the same as for the DTA experiment,  $\text{Al}_2\text{O}_3$  (Coors),  $\text{MgO}$  (Ozark Tech.), or Ta (homemade). For separating the grown crystals from the remaining liquid, a sieve was used. For the ceramic crucibles, an inverted crucible catches the liquid, while a plug of quartz wool in the catch crucible acted as a sieve. The Ta crucibles were ‘3-cap crucibles’ [3], with a built-in sieve. The crucibles were placed in a flat-bottom quartz ampoule with some quartz wool above and below the crucibles, to prevent possible cracking caused by differential thermal expansion between the quartz and the crucible and to provide cushioning during the decanting process. The quartz ampoule was evacuated and filled with a partial pressure of Ar, so that the pressure in the ampoule was nearly atmospheric at the highest temperature, and was then sealed. The ampoule was then placed in a box furnace, and subject to a heat treatment determined from DTA experiments (see Sec. 3). After the final temperature had been reached, the ampoule was taken out of the furnace, inverted into the cup of a centrifuge and quickly spun to decant the liquid from the crystals.

For initial characterization, we measured powder X-ray diffraction patterns on one or several finely ground crystals from the growth yield with a Rigaku Miniflex+ diffractometer employing  $\text{Cu-K}\alpha$  radiation. The patterns were analyzed with Rietica [6], using a Le Bail-type [7] of refinement.

### 3 Simulations

For the evaluation of measured DTA curves, we compared them to simulated, ideal, DTA curves. For the simulations, we considered a hypothetical binary system, the  $\alpha$ - $\delta$  system (Fig. 1). This system is composed of  $\alpha$  and  $\delta$  that melt congruently at  $700^\circ\text{C}$  and  $1000^\circ\text{C}$  or  $1400^\circ\text{C}$ , respectively, peritectic compounds  $\beta$  and  $\gamma$ , at  $\alpha_{50}\delta_{50}$  and  $\alpha_{25}\delta_{75}$ , respectively, and a eutectic alloy of composition  $\alpha_{15}\delta_{85}$  with a eutectic temperature of  $600^\circ\text{C}$ . At its decomposition temperature,  $800^\circ\text{C}$ , peritectic  $\beta$  decomposes into a liquid with composition  $\alpha_{60}\delta_{40}$  and solid  $\gamma$ , which in turn decomposes, at  $900^\circ\text{C}$ , into a liquid with

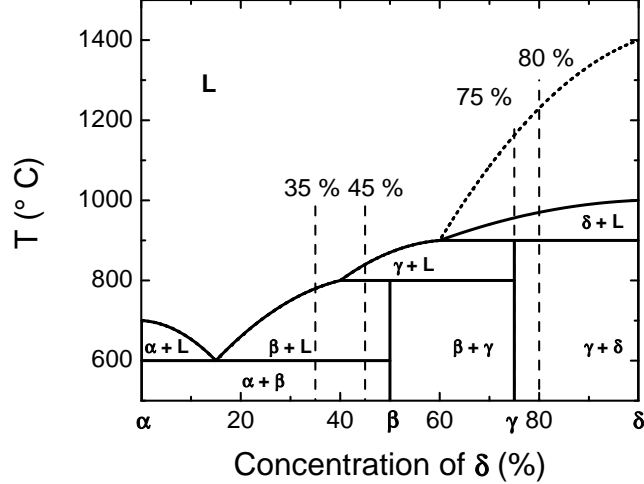


Fig. 1. Hypothetical binary phase diagrams containing two congruently melting phases,  $\alpha$  and  $\delta$  and two peritectics,  $\beta$  and  $\gamma$ . The dotted line is for  $\delta$  melting at 1400°C. The dashed vertical lines indicate compositions for which DTA curves were calculated.

composition  $\alpha_{40}\delta_{60}$  and solid  $\delta$ . For the liquidus lines we chose second-order polynomials with the concentration of  $\delta$  as a variable. This functional dependence can be considered realistic [8], and is easily evaluated.

A full discussion, see e.g. Ref. [9], of DTA is beyond the scope of this paper and we shall limit our consideration to a rather simple model. We will consider the DTA as a black box, that produces a signal proportional to the temperature derivative of the enthalpy of the sample. We assume that the enthalpies of formation for the phases  $\alpha$ ,  $\beta$ ,  $\gamma$ , and  $\delta$  are equal, and that the specific heats for the solid phases and the liquid (regardless of composition), are constant and equal. Then the simulated DTA signal is proportional to the temperature derivative of the fraction of solid to liquid, determined by the well-known lever law (see e.g. Ref. [10]). Our DTA measurements were usually carried out at heating and cooling rates of 10 to 40°C/min, which does not usually result in an equilibrium distribution of phases. Therefore, a cooling curve was calculated assuming that once a phase has solidified it does not dissolve back, or react with other solid phases. Then the composition of the liquid follows the liquidus line and the final solid contains a nonequilibrium distribution of phases. The calculated heating curve represents the heating curve of this nonequilibrium distribution of phases under the assumption that the kinetics are such that also during heating the liquidus line is followed. Although the assumptions are not fully realistic, the patterns recognizable in experimentally observed curves are reproduced well by our model.

During a DTA measurement (even in the absence of undercooling), there is a difference between the events observed in the heating and cooling curves. The melting and solidification events have the same onset temperature, but show a width (dependent on the heating or cooling rate). To include this effect in

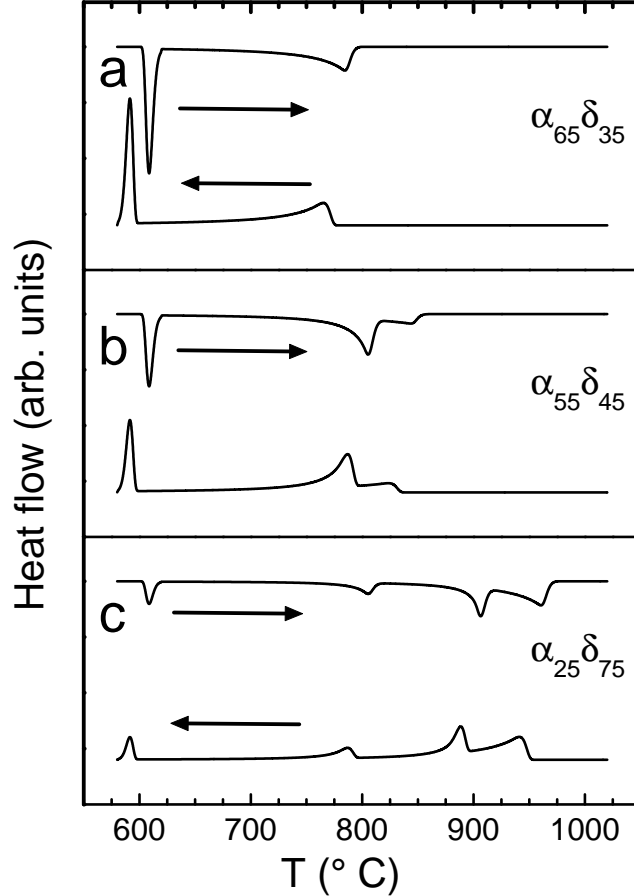


Fig. 2. Calculated DTA curves for various compositions of the phase diagram in Fig. 1. In each example, the lower curve is the cooling curve for a non-equilibrated sample, and the top curve is the heating curve for a non-equilibrated sample.

our simulations as an instrument response function, we assumed this temperature lag is temperature independent and can be described by the ‘standard  $\Gamma$  distribution’, that is often used to describe waiting times [11].

In Fig. 2a the calculated DTA curves for an alloy of composition  $\alpha_{65}\delta_{35}$  are presented (see dashed vertical line in Fig. 1). Events at both the eutectic ( $600^{\circ}\text{C}$ ) and liquidus ( $780^{\circ}\text{C}$ ) temperatures are clearly observed. The eutectic is a much more sharply defined event than the liquidus, because the observed thermal event is proportional to the temperature derivative of the fraction of solid-to-liquid. In Fig. 2b, the calculated DTA curves for an alloy of composition  $\alpha_{55}\delta_{45}$  are shown (see dashed vertical line in Fig. 1). The eutectic ( $600^{\circ}\text{C}$ ), and the peritectic decomposition of  $\beta$  ( $800^{\circ}\text{C}$ ) are clearly observed in the calculations, whereas the liquidus ( $840^{\circ}\text{C}$ ) is less obvious. In Fig. 2c, the calculated DTA curves for an alloy of composition  $\alpha_{25}\delta_{75}$  are shown for the case that  $\delta$  melts at  $1000^{\circ}\text{C}$  (see dashed vertical line in Fig. 1, crossing the lower-lying liquidus line). The eutectic ( $600^{\circ}\text{C}$ ), the peritectic temperature of  $\beta$  ( $800^{\circ}\text{C}$ ), the peritectic temperature of  $\gamma$  ( $900^{\circ}\text{C}$ ) and the liquidus ( $956^{\circ}\text{C}$ ) are visible.

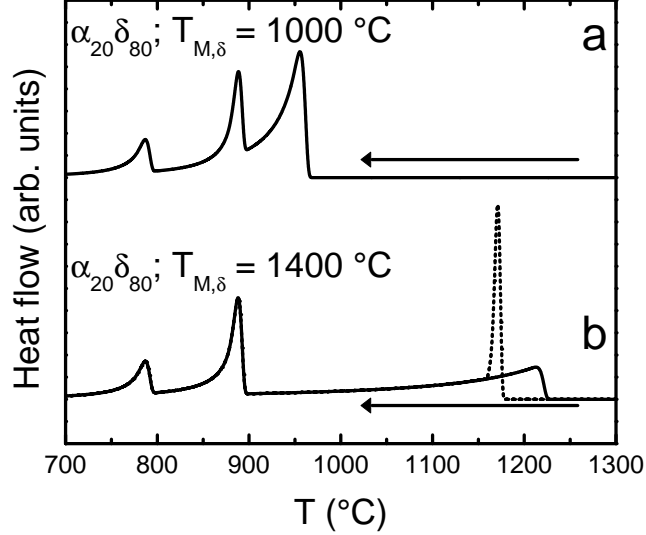


Fig. 3. Simulated DTA cooling curves for  $\alpha_{20}\delta_{80}$  of the phase diagram in Fig. 1, for (a)  $\delta$  melting at  $1000\text{ °C}$  and (b) at  $1400\text{ °C}$ . The dotted line in (b) represents a cooling curve with undercooling by  $50\text{ °C}$  taken into account.

Note that in the simulations for Figs. 2c the peritectic temperatures for the  $\beta$ -phase and the eutectic are visible because of the non-equilibrium nature of the model.

Such DTA curves can be used, especially in the case that the underlying phase diagram is unknown, to determine the temperature range over which crystals can be grown. For example, the DTA curves for a sample of composition  $\alpha_{65}\delta_{35}$  show that the primary solidification for that composition can be grown by slowly cooling between  $800\text{ °C}$  and  $600\text{ °C}$ . In addition, to separate the crystals from the liquid, the sample should be decanted above  $600\text{ °C}$ . After the growth, the crystals will be identified as  $\beta$ , e.g. by X-ray diffraction. Crystals of the  $\gamma$ -phase form for  $\alpha_{55}\delta_{45}$  and can be grown by slowly cooling between the liquidus,  $850\text{ °C}$ , and  $800\text{ °C}$ , and separated by decanting above  $800\text{ °C}$ . However, choosing the composition  $\alpha_{55}\delta_{45}$  is quite demanding: the maximum useful temperature range for growth is only about  $30\text{--}50\text{ °C}$ . Moreover, the weight fraction of crystals to liquid will be low for this composition. Finally, crystals of the  $\delta$ -phase form for  $\alpha_{25}\delta_{75}$  and can be grown (for the lower-lying liquidus line in Fig. 1) by cooling slowly between  $970\text{ °C}$ , and separated by decanting above  $900\text{ °C}$ .

The simulations indicate that the event associated with the liquidus can be quite weak (see Figs. 2a and b). As we mentioned above, the strength of the thermal signature for a liquidus is highly dependent on the slope of the liquidus curve, and can be very hard to detect experimentally. Consider an identical phase diagram, except that  $\delta$  melts at  $1400\text{ °C}$  (dotted in Fig. 1). As a result the liquidus curve above  $900\text{ °C}$  is considerably steeper. In Fig. 3, modelled DTA cooling curves for  $\alpha_{20}\delta_{80}$  alloys from both hypothetical systems are presented.

As can be seen, the DTA signature for the system with a lower-melting  $\delta$  and a lower slope is much easier to detect, i.e. removing more solid from the liquid per °C yields a stronger DTA signal.

Under the assumption that there is no time lag due to the dissolution of the last solid phase, the calculated heating curves can be considered realistic representations of actual measurements. However, experimental cooling curves may be shifted to lower temperatures due to undercooling. In many systems, the nucleation of the crystalline phase from the liquid can be slow. Since the DTA measurements were made at reasonably high cooling rates this may lead to significant undercooling. (note that in an actual growth experiment, typically at much slower cooling rates, there is probably less undercooling.) In an undercooled melt, when nucleation does occur, there is a rapid growth of the solid phase. In a simulation for the composition  $\alpha_{20}\delta_{80}$  with  $\delta$  melting at 1400°C, allowing undercooling by 50°C, the solidification is very clearly visible in the DTA curve (Fig. 3b, dotted line). Thus whereas we may not detect the true liquidus temperature we may be able to determine both an upper bound given by the maximum temperature to which the sample was heated, and a lower bound given by the solidification event for the liquidus. We can give the upper bound, because when not all crystals have been dissolved (i.e. the liquidus temperature has not been reached) these serve as perfect nucleation centers, preventing undercooling. Note that we have frequently observed that peritectic temperatures and occasionally the eutectic temperature are also undercooled.

## 4 Growth of TbAl

The growth of TbAl provides an example of the importance of identifying the right crucible material, and the role DTA measurements can play in this selection. Furthermore, it also provides an example of the efficient determination of a very narrow temperature range, by DTA, over which crystals can be grown.

The crystal structure and magnetic properties, that involve anisotropic exchange interactions, of polycrystalline TbAl were published some time ago [12,13,14,15]. For an estimate of a composition for the initial melt for solution growth, we considered the binary phase diagram of the Tb-Al system. To our knowledge, this has only been predicted [16,17], from the systematics of different rare-earth - Al binary systems, but not verified experimentally in detail. Especially the Tb-rich side (above  $\sim 56\%$  Tb) is uncertain. This predicted phase diagram includes 2 eutectics, at 3.5% (642°C) and at 77% Tb (903°C), and 5 compounds: TbAl<sub>3</sub>, TbAl<sub>2</sub>, TbAl, Tb<sub>3</sub>Al<sub>2</sub>, and Tb<sub>2</sub>Al. Of these, TbAl<sub>2</sub> melts congruently, whereas TbAl<sub>3</sub> and TbAl form peritectically. Even though Tb<sub>3</sub>Al<sub>2</sub> and Tb<sub>2</sub>Al are indicated to form peritectically as well, congruent melt-

ing cannot be excluded due to a lack of experimental data [16]. Since the phase diagram around this composition was indicated to be uncertain, a DTA experiment, rather than a slow and expensive growth served as an inexpensive and quick check, using only small amounts of starting materials. The primary-solidification line for TbAl reportedly lies between 57% and 67% Tb and 1079-986°C. Therefore, for the experiments described below, we chose to use an alloy with composition  $\text{Tb}_{60}\text{Al}_{40}$ .

In our experience, an alloy with more than 10-15% rare earth cannot be reliably held in an  $\text{Al}_2\text{O}_3$  crucible, because of thermite-type reactions. Furthermore, we considered it possible that the  $\text{Tb}_{60}\text{Al}_{40}$  alloy, being also rich in Al, would attack Ta, the other crucible material we regularly used in the past [1,2,3]. MgO, on the other hand, could be stable enough to use. To test the crucibles, we performed DTA experiments in the three available crucible materials:  $\text{Al}_2\text{O}_3$ , Ta, and MgO. In order to prevent direct contact of unreacted elements with the crucibles, we alloyed samples of approximately 40 mg by arc-melting prior to the DTA experiments. DTA heating and cooling cycles were performed three times between  $\sim 1240$  and  $\sim 600^\circ\text{C}$ , at heating rates of  $40^\circ\text{C}/\text{min}$  and cooling rates of  $10^\circ\text{C}/\text{min}$ . The curves obtained from the first two cycles, between  $800^\circ\text{C}$  and the highest temperature reached, are shown in Fig. 4.

Upon heating, in both the first and the second heating cycle, an endothermic event occurred near  $970^\circ\text{C}$  in all three cases. Besides a shift of the baseline, probably because the contact between the sample and the thermocouple changed after melting, the MgO and Ta-crucible curves show no significant difference between the first and second heating curves, and no clear events at higher temperatures. The two  $\text{Al}_2\text{O}_3$ -crucible heating curves, however, are very different: a clear exothermic bump between  $1070^\circ\text{C}$  and  $1120^\circ\text{C}$  is visible in the first heating curve, but not in the second one. Furthermore, the endothermic event near  $970^\circ\text{C}$  is less pronounced in the second heating curve, and followed by a pronounced second endothermic event that peaks near  $1100^\circ\text{C}$ .

Upon cooling, (note that the non-linear but smooth behavior at elevated temperatures in the cooling curves are due to stabilization of the furnace-ramp rate, rather than due to thermal events) the MgO and Ta-crucible curves show no significant difference between the first and the second cooling cycle. In the  $\text{Al}_2\text{O}_3$ -crucible curves, there are several differences between the first and second cooling curves. Particularly, near  $1210^\circ\text{C}$ , a weak exothermic event may be observed in the first cooling curve, but not in the second cooling curve. In both first and second cooling cycles, pronounced exothermic peaks were observed near  $1060^\circ\text{C}$  and  $960^\circ\text{C}$ . Note that the peak near  $1060^\circ\text{C}$  is *only* observed in the  $\text{Al}_2\text{O}_3$ -crucible curves.

These results are consistent with a thermite-type reaction of the alloy  $\text{Tb}_{60}\text{Al}_{40}$



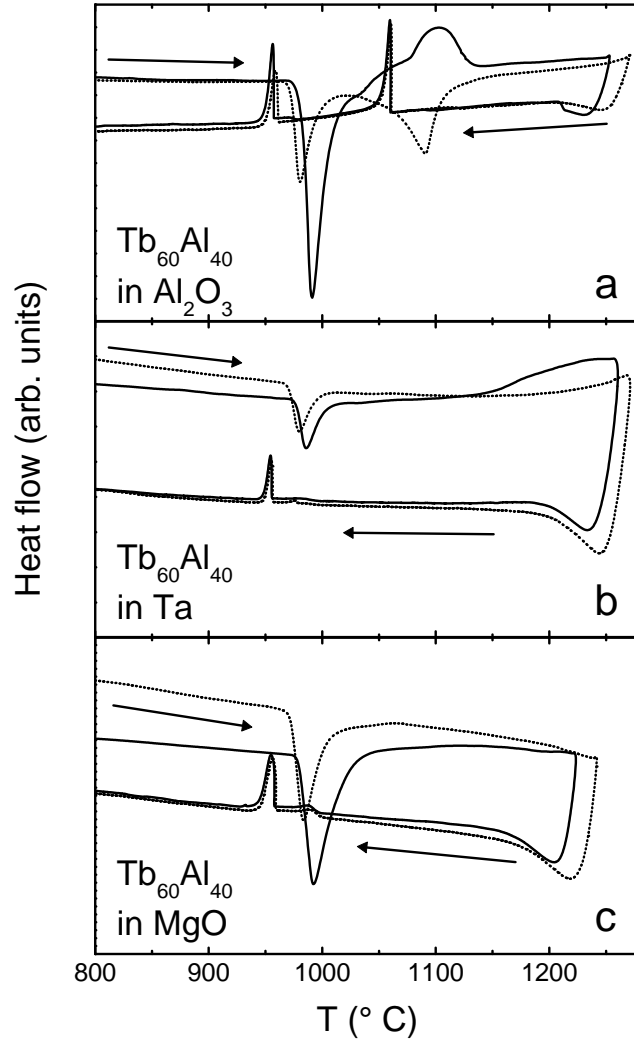


Fig. 4. The first (solid) and second (dotted) heating-and-cooling cycles of  $\text{Tb}_{60}\text{Al}_{40}$  in (a)  $\text{Al}_2\text{O}_3$ , (b) Ta, and (c) MgO, measured upon heating with a  $40^\circ\text{C}/\text{min}$  rate and cooling with a  $10^\circ\text{C}/\text{min}$  rate.

with the  $\text{Al}_2\text{O}_3$  crucible, reducing the amount of Tb in the metallic liquid, and increasing the amount of Al. The exothermic bump in the first heating cycle, between  $1080$  and  $1120^\circ\text{C}$  (Fig. 4a) then is associated with this reaction. The event that occurred upon cooling at  $1060^\circ\text{C}$ , is likely due to the peritectic temperature of  $\text{TbAl}$ , predicted to be at  $1079^\circ\text{C}$  [16,17]. Furthermore, the highest-temperature event in the first cooling cycle was no longer present in the second cooling cycle, maybe due to the sample becoming so rich in Al that it could no longer fully melt (the nearest compound richer in Al,  $\text{Al}_2\text{Tb}$  reportedly melts at  $1514^\circ\text{C}$ ).

Since both Ta and MgO showed no evidence of a reaction, both are good candidates as a crucible material. (Although we worried that the  $\text{Tb}_{60}\text{Al}_{40}$  alloy would attack Ta, there is no clear indication of such an attack from the DTA results.) For the growth experiment, we chose MgO as the crucible

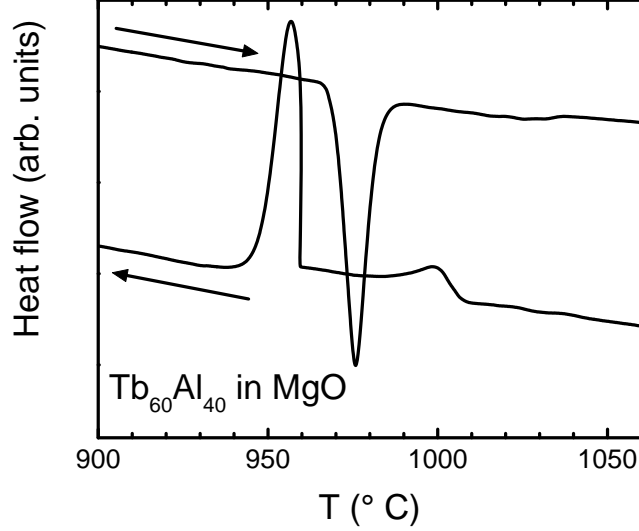


Fig. 5. Relevant part of the DTA curve of our sample of  $Tb_{60}Al_{40}$  measured upon heating with a  $10^{\circ}C/min$  rate and cooling with a  $10^{\circ}C/min$  rate.

material.

The heat treatment for the growth experiment is determined from the details of the DTA curves. In Fig. 5, the relevant parts of a third heating and cooling curve (measured at  $10^{\circ}C/min$  for both heating and cooling) are shown for an  $MgO$ -crucible experiment. Upon heating, a sharp endothermic peak is observed with an onset temperature of about  $965^{\circ}C$ . This is followed by a weak step near  $1015$ - $1035^{\circ}C$ . Upon cooling, two events are observed. There is a weak exothermic bump with an onset temperature of about  $1010^{\circ}C$ , followed by a strong exothermic peak with an onset temperature of about  $960^{\circ}C$ . Note the resemblance between these experimental results and the simulation in Fig. 2a, and also note that there is some undercooling of the liquidus,  $\sim 5$ - $30^{\circ}C$ , that makes the liquidus much more visible upon cooling, as in the simulation in Fig. 3. The measurements suggest that crystals of the primarily solidifying compound for the composition  $Tb_{60}Al_{40}$  can be grown by cooling slowly between  $\sim 1020^{\circ}C$  and  $\sim 965^{\circ}C$ , followed by a decant above  $\sim 965^{\circ}C$ . Taking into account the possibility of undercooling, this heat treatment is very demanding (limited temperature range for growth), and may be influenced by differences in thermometry between the growth furnace and the DTA.

For the growth experiment, an arc-melted button ( $\sim 3$  g) was first heated to  $1200^{\circ}C$ , kept at this temperature for 2 h for homogenization, then it was cooled in  $\sim 1$  h to  $1020^{\circ}C$ , near the observed liquidus in the heating curve of the DTA experiment. Finally, it was cooled in 10 h to  $975^{\circ}C$ , which is near the temperature of the onset of the endothermic event in the heating curve of the DTA experiment. At this temperature, the sample was decanted. In the growth crucible, large crystals of several mm were found (see the photograph in Fig. 6a). Powder-X-ray diffraction identifies the crystals as  $TbAl$ , with space

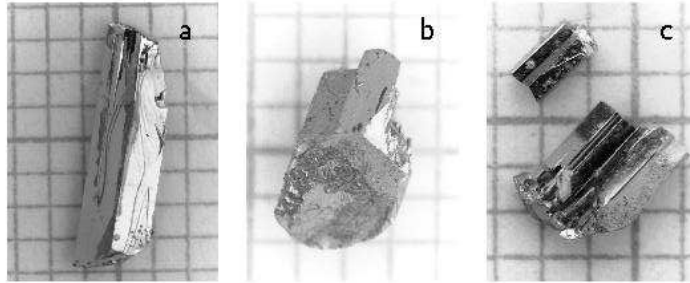


Fig. 6. Photographs of the crystals of which the growth is described in the text. From left to right: (a) TbAl, (b) Pr<sub>7</sub>Ni<sub>2</sub>Si<sub>5</sub>, (c) YMn<sub>4</sub>Al<sub>8</sub>. In each case a mm grid was used as a background.

group *Pbcm*, and lattice parameters  $a=5.85(3)$  Å,  $b=11.4(3)$  Å, and  $c=5.63(3)$  Å, in agreement with the reported crystal structure [12].

Crystals of TbAl could probably have been obtained from the alloy Tb<sub>60</sub>Al<sub>40</sub> based upon the available binary phase diagram alone, cooling slowly below the reported liquidus temperature ( $\sim 1060^\circ\text{C}$ ) and decanting above the reported peritectic temperature for Tb<sub>3</sub>Al<sub>2</sub> ( $986^\circ\text{C}$ ). However, we have often observed that binary phase diagrams with rare-earth components need revision (see e.g. [18]), and the Tb-Al binary phase diagram was already known to be uncertain [16,17].

For the DTA simulations, we have assumed that the solidification of an alloy follows the liquidus. Under these assumptions, it seems from our DTA experiments on Tb<sub>60</sub>Al<sub>40</sub>, that the solidification of TbAl is immediately followed by a last, eutectic, solidification at a temperature substantially higher than the eutectic temperature reported ( $903^\circ\text{C}$ ). If the alloy indeed followed the liquidus, the published binary phase diagram [16] requires re-examination. However, further experiments, which are outside the scope of this paper, would be required to clarify this.

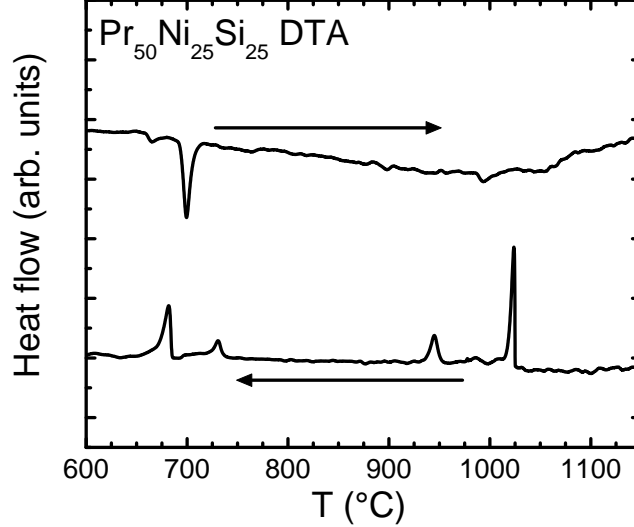


Fig. 7. Relevant part of the DTA curve of our sample of  $\text{Pr}_{50}\text{Ni}_{25}\text{Si}_{25}$  measured upon heating and cooling with a  $10^\circ\text{C}/\text{min}$  rate.

## 5 Growth of $\text{Pr}_7\text{Ni}_2\text{Si}_5$

We are currently investigating the ternary Pr-Ni-Si system, including the liquidus surface of the Pr-rich corner. Approximately 20 ternary intermetallic compounds have been reported [18] for the Pr-Ni-Si system, in accordance with what was reported for Ce-Ni-Si [19], and Nd-Ni-Si [20]. One of those is the compound  $\text{Pr}_7\text{Ni}_2\text{Si}_5$ .

For many Pr-Ni-Si compounds, the range of compositions that form the primary-solidification surface is very narrow, sometimes down to a few percent [21]. Therefore, it is useful to quickly and systematically test different compositions via DTA analysis. In this section, we show that our DTA and growth experiments, on an alloy of composition  $\text{Pr}_{50}\text{Ni}_{25}\text{Si}_{25}$ , resulted in the identification and optimized growth of the compound that solidifies primarily:  $\text{Pr}_7\text{Ni}_2\text{Si}_5$ .

A rod of several grams of composition  $\text{Pr}_{50}\text{Ni}_{25}\text{Si}_{25}$  was prepared by arc-melting and drop-casting. Since the rod had cooled down very quickly, we considered it homogeneous on the scale of the DTA samples. Therefore, a piece of this rod, of the typical size for a DTA experiment or a growth, was considered representative for the whole rod. Two pieces were taken, about 40 mg for the DTA experiment, and about 2.25 g for the growth experiment.

For the experiments, we used Ta crucibles as experience showed us that, whereas Ta may be expected to be attacked by Ni and Si [22], these alloys (with about 50% of Pr) do not appear to attack the crucible.

For the DTA experiment, the sample was heated and cooled three times be-

tween  $\sim 400$  and  $\sim 1200^\circ\text{C}$  at  $10^\circ\text{C}/\text{min}$ . After the first heating cycle, during which the sample settled in the crucible, the measurements were reproducible. In Fig. 7, the relevant parts of the third-cycle curves are shown. The curves are substantially noisier than those shown for the TbAl experiment. This may be because the thermal contact between the Ta crucible and its ceramic liner varied, or because the mass of the Ta crucible was substantially greater than that of the sample inside it. In spite of the noise, we were able to extract information, useful for crystal growth, from the experiment.

In the cooling curve, four sharp exothermic events can be observed, with onset temperatures of about  $1025^\circ\text{C}$ ,  $950^\circ\text{C}$ ,  $730^\circ\text{C}$ , and  $685^\circ\text{C}$ . This experimental cooling curve can roughly be compared to the simulation of the hypothetical binary alloy  $\alpha_{25}\delta_{75}$ , see Fig. 2c. In that simulation, upon cooling, four events occur, the liquidus, two events associated with peritectics, and the eutectic. The experimental liquidus is probably sharpened by undercooling, see Fig. 3. In the experimental heating curve, only one event with an onset temperature of about  $690^\circ\text{C}$ , can be observed clearly. At higher temperatures, there may be an event near  $990^\circ\text{C}$  (a weak peak), and between  $\sim 1050$ - $1090^\circ$  (a broad step).

Note that, whereas we do not fully understand the differences between these heating and cooling curves (particularly in the lower temperature range), for crystal growth we only need to know the temperature region over which only the primary solidification grows, i.e. between the liquidus temperature and the temperature where secondary phases may start to grow.

The heat treatment for crystal growth might be proposed based upon the DTA cooling curve alone, but we used the heating curve for some guidance. For estimation of the liquidus, we examined at the highest-temperature events. In the cooling curve, the shape of the peak near  $1025^\circ\text{C}$  appears consistent with undercooling (c.f. Fig. 3b). In the heating curve, the broad step between  $\sim 1050$ - $1090^\circ$  may be associated with that peak and appears similar to the simulated liquidus in Fig. 2b. In the cooling curve, the second-highest temperature event appears as a sharp peak near  $940^\circ$  suggesting a decanting temperature higher than  $940^\circ$  (but lower than  $1025^\circ$ ). The weak peak in the heating curve at  $990^\circ$  may suggest that secondary phases can start to grow below that temperature. Since this temperature falls between the two highest-temperature events in the cooling curve, we considered it safe to decant at a temperature slightly above  $990^\circ$ . Therefore, we used the following heat treatment for the growth experiment. The sample was heated to  $1190^\circ\text{C}$  in 5 h, and allowed to equilibrate for 2 h. After that, it was cooled to  $1100^\circ\text{C}$  in 2 h. After this it was cooled to  $1000^\circ\text{C}$  in 50 h, after which the sample was decanted. In the crucible, large mm-sized blocky crystals were found. A photograph of one of the crystals is displayed in Fig. 6b.

Powder-X-ray diffraction identified the crystals as  $\text{Pr}_7\text{Ni}_2\text{Si}_5$ , with space group is  $Pnma$ , and lattice parameters  $a=23.32(3)$  Å,  $b=4.302(3)$  Å, and  $c=13.84(3)$  Å, in agreement with the reported crystal structure [23]. The compound is only known by its crystal structure, therefore we are currently investigating its low-temperature thermodynamic and transport properties [24]. The combined DTA and crystal-growth experiments demonstrate that composition  $\text{Pr}_{50}\text{Ni}_{25}\text{Si}_{25}$  is part of the primary phase field of the compound  $\text{Pr}_7\text{Ni}_2\text{Si}_5$ .

## 6 Growth of $\text{YMn}_4\text{Al}_8$ (and $\text{YMn}_2\text{Al}_{10}$ )

The growth of  $\text{YMn}_4\text{Al}_8$  provides an example of how DTA can help make finding the right composition for solution growth very efficient. The ternary intermetallic compound  $\text{YMn}_4\text{Al}_8$  has been known at least since 1971 [25], but has only been synthesized in polycrystalline form. Recently [26], it was reported that  $\text{YMn}_4\text{Al}_8$  has a narrow pseudogap in the spin excitation spectrum. This prompted us to try to grow single crystals.

The published partial triangulated ternary isotherm for the Y-Mn-Al system [25] at  $600^\circ\text{C}$  suggests that a growth may be attempted from an Al-rich liquid. Therefore, we tried to grow it using a composition approximately halfway between Al and  $\text{YMn}_4\text{Al}_8$ :  $\text{Y}_{36}\text{Mn}_{145}\text{Al}_{819}$ . We chose an  $\text{Al}_2\text{O}_3$  crucible, since in our experience such an alloy will likely not attack it, and we started with pieces of the elements. The sample was cooled in 15 h between  $\sim 1200^\circ\text{C}$  and  $950^\circ\text{C}$ , then decanted. The mm-sized prismatic crystals in the growth crucible were identified as  $\text{YMn}_2\text{Al}_{10}$ , which was not reported in the ternary isotherm, but does appear in literature [27].

As a next step, we alloyed by arc-melting a total of about 1 g of the starting elements in the  $\text{YMn}_4\text{Al}_8$  ratio. Although we had some losses due to evaporation of Mn, about 2%, after arc melting, an X-ray powder diffraction experiment indicated the sample to be mainly  $\text{YMn}_4\text{Al}_8$ . Then we performed DTA, in an  $\text{Al}_2\text{O}_3$  crucible, on a  $\sim 20$  mg piece. Up to  $1350^\circ\text{C}$  there was only one noticeable thermal event in both the heating and cooling curves, at temperatures between  $1220$ - $1240^\circ\text{C}$ . This, combined with the diffraction, is an indication that  $\text{YMn}_4\text{Al}_8$  is congruently melting at  $1220$ - $1240^\circ\text{C}$ .

A congruently melting material is part of its own primary solidification surface. Therefore, we decided to try a composition nearby  $\text{YMn}_4\text{Al}_8$ . The melting temperature of the desired phase is higher than the reported liquidus temperature for an alloy of composition  $\text{Mn}_4\text{Al}_8$ ,  $\sim 1100^\circ\text{C}$  [28], therefore it seemed possible to grow  $\text{YMn}_4\text{Al}_8$  out of a composition close to the binary Mn-Al-line.

We decided to try an alloy of composition  $\text{Y}_4\text{Mn}_{32}\text{Al}_{64}$  using  $\text{Al}_2\text{O}_3$  crucibles.

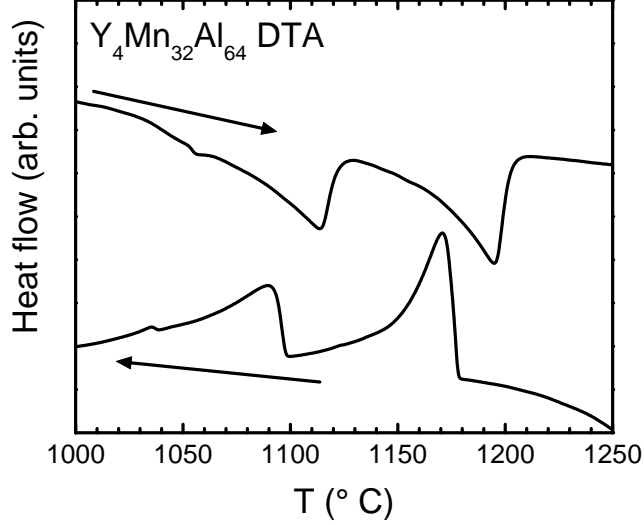


Fig. 8. Relevant part of the DTA curve of our sample of  $Y_4Mn_{32}Al_{64}$  measured upon heating and cooling with a  $20^\circ\text{C}/\text{min}$  rate.

We alloyed a few grams by arc-melting, and again had losses (about 3%) due to Mn evaporation. In order to make a small sample representative for the whole, the arc-melted button was coarsely ground and the powder thoroughly mixed. About 20 mg of the powder was used for a DTA experiment. The results for heating and cooling at  $20^\circ\text{C}/\text{min}$ , between 1000 and  $1250^\circ\text{C}$ , are shown in Fig. 8. In both the heating and the cooling curve, two very pronounced events are visible. In the heating curve, peaks are seen near  $1110^\circ\text{C}$  and  $1200^\circ\text{C}$ , while in the cooling curve events occur at onset temperatures of  $\sim 1180^\circ\text{C}$  and  $\sim 1100^\circ\text{C}$ . A weak event is observed at lower temperatures of  $1030\text{--}1050^\circ\text{C}$  in both the heating and cooling curve. For the determination of growth parameters only the two highest-temperature events are important, therefore we did not measure down to still lower temperatures. These experimental curves can be compared to the simulated curves in Fig. 2c.

The DTA experiment suggests that crystals can be grown and separated from the remaining melt by cooling an alloy of composition  $Y_4Mn_{32}Al_{64}$  slowly below  $\sim 1200^\circ\text{C}$  (above the highest-temperature peak in the heating curve) and decanting above  $\sim 1130^\circ\text{C}$  (above the second-highest-temperature peak in the heating curve). For a growth experiment, we started with appropriate amounts of pieces of the elements. The sample was first heated to  $1250^\circ\text{C}$  for equilibration, and then cooled in 1 h to  $1200^\circ\text{C}$ , below which it was cooled to  $1160^\circ\text{C}$  in 60 h. At this temperature the sample was decanted. Well-separated prismatic crystals were found in the growth crucible. A photograph of two of those crystals is presented in Fig. 6c. Powder-X-ray diffraction identified the crystals as  $Y\text{Mn}_4\text{Al}_8$ , with space group  $I4mmm$ , and lattice parameters  $a=8.86(1)\text{ \AA}$ ,  $c=5.12(1)\text{ \AA}$ , in agreement with the reported crystal structure [29].

## 7 Summary and conclusions

The examples presented here address how DTA can help in determining growth parameters for solution growth, without detailed knowledge of phase diagrams. As shown with the example of TbAl, DTA can sometimes help in identifying the right crucible material, and, moreover, it can help pinpointing a very narrow temperature range over which to grow crystals. The example of the growth of  $\text{Pr}_7\text{Ni}_2\text{Si}_5$  shows that the combination of DTA and growth experiments can help in determining the primarily solidifying compound out of a given metallic liquid, while limiting the growth to that of the primary. Finally, the example of  $\text{YMn}_4\text{Al}_8$  shows how DTA can help in the quick determination of the primary phase field for a compound.

Extensions of the method can be sought in including other crucible materials for DTA, e.g. BN. Or, in order to reduce problems with elements that have high vapor pressures, in sealing the Ta-DTA crucibles. However, problems still exist with elements that have a high vapor pressure and cannot be held in Ta.

As was already discussed by Fisk and Remeika [1], one of the great advantages of solution growth is the economy of the method. By including DTA in the procedure to optimize growth, it can be economized even further, especially in terms of material costs. Furthermore, although DTA generally shows that “something occurs at a certain temperature” [4], the combination of a DTA experiment with a growth experiment, if successful, can lead to definite conclusions regarding the primarily solidifying compound out of a metallic liquid of certain composition. For this it is not necessary to establish a full phase diagram, a DTA experiment on a sample of the composition of interest is sufficient.

## 8 Acknowledgements

The authors wish to thank J. Fredericks, S. Chen, B. K. Cho, M. Huang, D. Wu, T. A. Lograsso, S. L. Bud'ko, G. Lapertot for their kind help in discussing and preparing samples. The financial support from the US Department of Energy is gratefully acknowledged: Ames Laboratory is operated for the US Department of Energy by Iowa State University under Contract No. W-7405-Eng-82. This work was supported by the Director for Energy Research, Office of Basic Energy Sciences.



## References

- [1] Z. Fisk, J. P. Remeika, in: K. A. Gscheidner, Jr., L. Eyring (Eds.), Handbook on the Physics and Chemistry of Rare Earths, Vol. 12, Elsevier, Amsterdam, 1989.
- [2] P. C. Canfield, Z. Fisk, Philos. Mag. B 65 (1992) 1117.
- [3] P. C. Canfield, I. R. Fisher, J. Cryst. Growth 225 (2001) 155.
- [4] D. Schultze, Thermochem. Acta 190 (1991) 77.
- [5] F. W. Wilburn, J. Sci. Instrum. 35 (1958) 403.
- [6] B. Hunter, Lhpm-rietica, [www.rietica.org](http://www.rietica.org).
- [7] A. Le Bail, H. Duroy, J. L. Fourquet, Mater. Res. Bull. 23 (1988) 447.
- [8] H. Okamoto, T. B. Massalski, J. Phase Equilib. 12 (1991) 148.
- [9] W. J. Boettinger, U. R. Kattner, Metall. Mater. Trans. A 33A (2002) 1779.
- [10] J. D. Verhoeven, Fundamentals of Physical Metallurgy, J. Wiley and Sons, New York, 1975.
- [11] R. V. Hogg, A. Craig, Introduction to Mathematical Statistics, Macmillan, New York, 1966.
- [12] C. Bècle, R. Lemaire, Acta Crystallogr. 23 (1967) 840.
- [13] B. Barbara, C. Bècle, R. Lemaire, R. Pauthenet, J. Appl. Phys. 39 (1968) 1084.
- [14] C. Bècle, R. Lemaire, E. Parthe, Solid State Commun. 6 (1968) 115.
- [15] C. Bècle, R. Lemaire, D. Paccard, J. Appl. Phys. 41 (1970) 855.
- [16] R. Ferro, S. Delfino, G. Borzone, A. Saccone, G. Cacciamani, J. Phase Equilib. 14 (1993) 273.
- [17] R. Ferro, S. Delfino, G. Borzone, A. Saccone, G. Cacciamani, J. Phase Equilib. 15 (1994) 125.
- [18] M. Huang, T. A. Lograsso, J. Alloys Compd. 395 (2005) 75.
- [19] P. Rogl, in: K. A. Gscheidner, Jr., L. Eyring (Eds.), Handbook on the Physics and Chemistry of Rare Earths, Vol. 7, Elsevier, Amsterdam, 1984.
- [20] O. Bodak, P. Salamakha, O. Sologub, J. Alloys Compd. 256 (1997) L8.
- [21] M. Huang, unpublished.
- [22] F. R. de Boer, R. Boom, W. C. M. Mattens, A. R. Miedema, A. K. Niessen, in: F. R. de Boer, D. G. Pettifor (Eds.), Cohesion in Metals, Transition Metal Alloys, Vol. 1, Elsevier, Amsterdam, 1988.

- [23] M. Mys'kiv, O. Bodak, E. I. Gladyshevskii, in: R. Rykhal (Ed.), Tezisy Dokl. Vses. Konf. Kristallokhim. Intermet. Soedin. 2nd Ed., 1974, p. 31.
- [24] Y. Janssen et al., unpublished.
- [25] R. M. Rykhal, O. S. Zarechnyuk, N. V. German, Russ. Metall.-Metall.-U. 6 (1971) 205.
- [26] H. Nakamura, S. Giri, T. Kohara, J. Phys. Soc. Jpn. 73 (2004) 2971.
- [27] V. M. T. Thiede, W. Jeitschko, Z. Naturforsch. B 53 (1998) 673.
- [28] A. Jansson, Metall. Trans. A 23 (1992) 2953.
- [29] K. H. J. Buschow, J. H. N. van Vucht, W. W. van den Hoogenhof, J. Less-Common Met. 50 (1976) 145.